The Formation Conditions and Sources of Ore-Forming Fluids of the Nikolaevskoe Gold Deposit (South Urals)

S.E. Znamenskii[a, ✉], N.N. Ankusheva[b,c], A.V. Snachev[a]

[a] *Institute of Geology, Ufa Federal Research Center of the Russian Academy of Sciences, ul. K. Marksa 16/2, Ufa, 450077, Russia*

[b] *Institute of Mineralogy, South Urals Federal Research Center of Mineralogy and Geoecology,*
Ural Branch of the Russian Academy of Sciences, Ilmensky Reserve 1, Miass, 456317, Russia

[c] *South Ural State University, ul. 8 Iyulya 10, Miass, 456304, Russia*

Abstract—We studied fluid inclusions, trace elements, and oxygen, carbon, and sulfur isotope ratios in minerals from stockwork sulfide–carbonate–quartz ores of the Nikolaevskoe gold deposit confined to volcanic island arc porphyry intrusions. The study shows that fluid inclusions in quartz were homogenized at 260–200 ºC and those in later formed calcite, at 227–205 ºC. The fluids contain aqueous K–Mg–Na chloride solutions with salinity of 4.1–9.6 wt.% NaCl eq. Raman spectroscopy revealed CO_2 (29–34 mol.%), CH_4 (40–55 mol.%), and N_2 (8–30 mol.%) in the fluids. According to LA-ICP-MS data, quartz has low contents of Al (11.7–102 ppm) and Ti (0.05–0.64 ppm), which indicates its deposition from weakly acid low-alumina fluids at <350 ºC. The REE patterns of calcite show accumulation of heavy lanthanides ($La_N/Yb_N = 0.2$–0.9), evident of high fluid alkalinity, and negative Ce (0.39–0.82) and positive Eu (1.99–5.25) anomalies. The negative Ce anomalies are due to meteoric water in the fluid and the fluid interaction with limestones. The positive Eu anomalies reflect the high-temperature (>250 ºC) environment that existed before the calcite crystallization. The Y/Ho ratio in calcite (28.7–54.1) suggests that the fluid has magmatic components and components extracted from limestones and contains seawater. The $\delta^{18}O_{H_2O}$ values (3.6–5.6‰) of the fluid testify to the participation of magmatic and meteoric waters in the ore formation. The $\delta^{13}C_{CO_2}$ values (–4.1 to 1.4‰) point to carbon of magmatic nature and carbon extracted from limestones. The heavy sulfur isotope composition of pyrite (6.75 to 9.87‰) and arsenopyrite (8.7‰) might be due to sulfur supply from the host rocks or to the participation of $[SO_4]^{2-}$ of seawater in the ore-forming process. According to the results obtained, the Nikolaevskoe gold deposit is an island arc (Au ± Cu)–quartz–sulfide deposit transitional between porphyry and epithermal types.

Keywords: porphyry gold deposit, fluid inclusions, REE, carbon, oxygen, and sulfur isotopes, South Urals

INTRODUCTION

The Nikolaevskoe deposit is confined to the Main Uralian Fault (MUF) zone, to the northern closure of the Magnitogorsk megazone of the South Urals (Fig. 1). According to the spatial association with island arc porphyry intrusions, the stockwork morphology of the orebodies, and the propylitic composition of metasomatic wallrocks, it is assigned to porphyry gold deposits, which are rare in the Urals (Znamenskiy and Holodnov, 2018). The sources, *P–T* parameters, and composition of mineral-forming fluids of the deposit have not been studied until recently.

According to Sillitoe (2010), gold in porphyry copper (porphyry-epithermal (Kovalenker, 2003)) ore-forming systems is concentrated at different depths. Gold mineralization can occur in ores of porphyry and skarn deposits forming in

hypabyssal conditions. In subvolcanic settings it is confined to various epithermal objects. Gold is also present in vein polymetallic and quartz–sulfide deposits transitional between porphyry and epithermal types (Corbett and Leach, 1998). Sillitoe (2010) proposed to title them subepithermal. Carbonate rocks located far from porphyry intrusions often bear hydrothermal–metasomatic Zn–Pb–Ag ± Au (Cu) mineralization. Elucidation of the factors responsible for the formation of various types of gold mineralization in epithermal porphyry systems is an urgent problem.

The Nikolaevskoe deposit, like most of porphyry Cu (± Au, Mo) deposits in the Magnitogorsk megazone, fits the diorite model of porphyry systems (Grabezhev et al., 2017). At the same time, it differs significantly from other porphyry objects in the petrological and geochemical features of ore-bearing intrusions and in the geodynamic settings of formation. According to modern concepts (Plotinskaya et al., 2017), porphyry Cu (± Au, Mo) deposits in the Magnitogorsk megazone formed at two stages of evolution: (1) island arc formation in the Middle Devonian (Salavatskoe and

✉Corresponding author.
E-mail address: Znamensky_Sergey@mail.ru (S.E. Znamenskii)
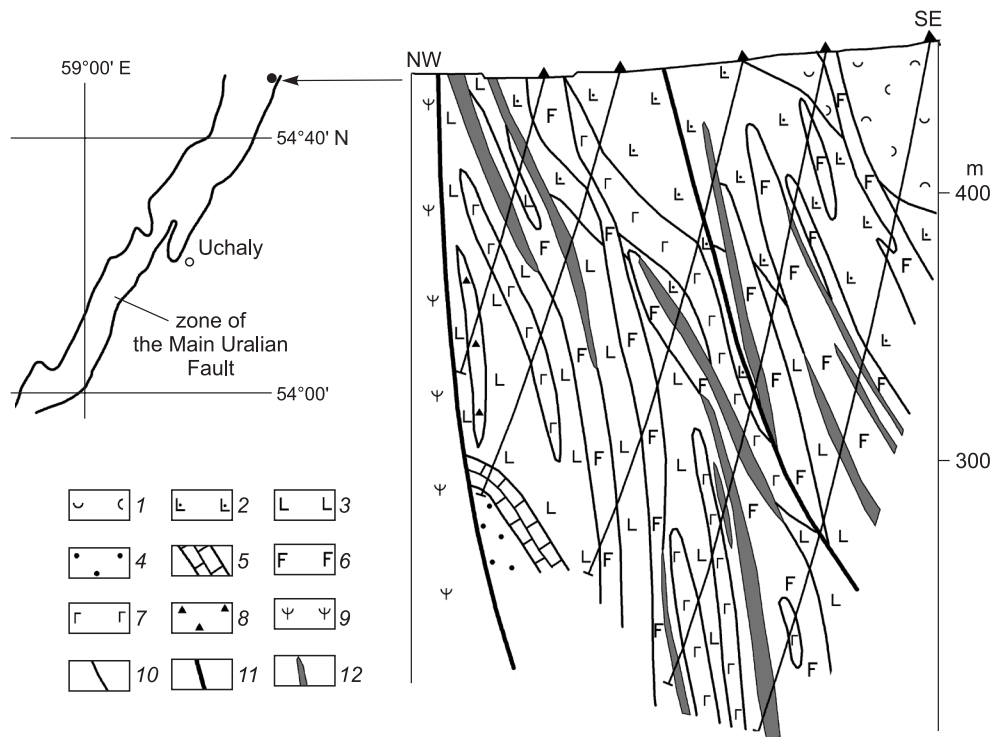
Fig. 1. Geologic section of the Nikolaevskoe gold deposit along the N-7 profile (after data from the Uchaly Department of OAO Bashkirgeologiya). *1*, layered mafic tuffs and tephroids; *2*, pyroxene–plagiophyre or, sometimes, plagiophyre basalts and their tuffs; *3*, plagiophyre basalts with subordinate interbeds of mafic tuffs; *4*, clay–siliceous shales, volcanomict siltstones, sandstones, and gritstones; *5*, biogenic limestones; *6*, dolerite–porphyrite and gabbro–diorite–porphyrite dikes; *7*, gabbro; *8*, magmatogene breccias of gabbro–diorite–porphyrites; *9*, serpentinites; *10*, geologic borders; *11*, faults; *12*, orebodies.

Voznesenskoe porphyry Cu, Mednogorskoe porphyry Cu–Au, and other deposits); (2) early collision of the Devonian island arc with the margin of the East European Platform in the Late Devonian–early Carboniferous (Yubileinoe porphyry Au deposit, Verkhneuralskoe and Mossovskoe porphyry Mo ore occurrences). Productive granitoid intrusions, except for subalkalic massifs with porphyry Mo mineralization, usually have a calc-alkalic composition (Grabezhev, 2009).

The Nikolaevskoe deposit is confined to a volcano-intrusive island arc association uniting low-K igneous, mostly mafic, rocks of tholeiitic and tholeiitic-calc-alkalic transitional series (Znamenskiy and Holodnov, 2018). In geochemical parameters the rocks of the gold-bearing assemblage are similar to the volcanics of the Baimak–Buribai Formation (D_1e_2), dated from conodonts at many sites in the northern part of the MUF zone (Maslov and Artyushkova, 2010), and are their age analogues. Volcanic complexes of the Baimak–Buribai Formation, composing the frontal paleo-island arc (Kosarev et al., 2005), host volcanogenic massive sulfide (VMS) deposits in the southern regions of the Magnitogorsk megazone (Gai, Bakr-Tau, etc.). The Nikolaevskoe deposit formed presumably in the junction zone of the northern closure of the frontal arc and the back-arc basin (Znamenskiy and Holodnov, 2018). In the late Emsian, this zone was in the relative-compression setting favorable for the formation of porphyry mineralization (Sillitoe, 2000).

To elucidate the *P–T* conditions of formation of gold mineralization in VMS ore-bearing complexes and the composition and possible sources of mineral-forming fluids, we studied fluid inclusions, trace elements, and carbon, oxygen, and sulfur isotope ratios in ore minerals from the Nikolaevskoe deposit.

A BRIEF GEOLOGICAL OUTLINE OF THE DEPOSIT

The Nikolaevskoe deposit occurs in a tectonic block of sedimentary and volcanic rocks localized among melanged serpentinites. The basement of the ore-hosting section is formed by a member of laminated clay-siliceous shales, limestones, and volcanomict rocks (Fig. 1). The overlying bed is made up of plagiophyre and pyroxene–plagiophyre basalts and mafic tuffs and tephroids. Stratified deposits are intruded by coarse-grained gabbro bodies and numerous younger dikes of plagiophyre dolerite-porphyrites, fine-grained gabbro–diorite–porphyrites, and their magmatogene breccias. Effusive and intrusive rocks with geochemical characteristics of suprasubductional rocks have a similar chemical composition and are united into a volcano-intrusive association (Znamenskiy and Holodnov, 2018).

The orebodies of the Nikolaevskoe deposit are linear sulfide–carbonate–quartz stockworks (Fig. 2) localized mostly
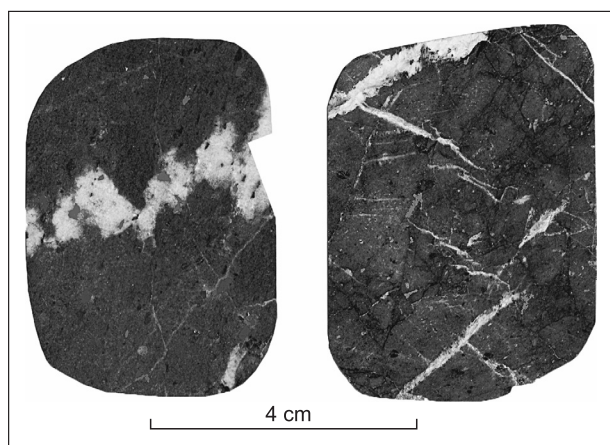
Fig. 2. Veinlet sulfide–carbonate–quartz ores from the Nikolaevskoe deposit.

in endo- and exocontact zones of dolerite–porphyrite and gabbro–diorite-porphyrite dikes and magmatogene breccias. An LA-ICP-MS analysis showed that the carbonate in ore veinlets is calcite (CaO = 51.9–56.38, MgO = 0.05–0.13, FeO = 0.07–0.18, MnO = 0.25–0.6, SrO = 0.13–0.43, BaO $\leq$ 0.0005, PbO $\leq$ 0.0002, and ZnO $\leq$ 0.0001 wt.%, n = 14 (number of analyses)). The hosted sulfides are dominated by pyrite. Pyrrhotite, arsenopyrite, chalcopyrite, sphalerite, galena, finely dispersed native gold, and, probably, tennantite are subordinate. The total content of sulfides does not exceed 10 vol.%.

Ore-bearing rocks, including dikes, underwent pre-ore propylitization (association of actinolite, epidote, chlorite, and pyrite) (Fig. 3). Such metasomatic alteration takes place at temperatures above 300 ºC (Zharikov, 1998). Gold ore mineralization is accompanied by propylites of the lower-temperature albite–chlorite facies. The metasomatic wallrocks contain albite, chlorite, calcite, quartz, prehnite, and, in places, sericite and biotite. According to Grabezhev and Belgorodskii (1992), propylite-type metasomatites are a distinctive feature of porphyry deposits localized in low-K granitoids in the MUF zone.

Post-ore quartz–carbonate and carbonate veinlets are widespread in the Nikolaevskoe deposit. The ore-bearing section is disturbed by thrusts formed apparently in the late Paleozoic, at the collision stage of the MUF zone evolution.

According to the results of exploration by OAO Bashkirgeologiya in 2007–2009, the resources of gold of grade P_1 in the Nikolaevskoe deposit are predicted to be 9.5 tons, and the average gold content is estimated at 6.01 ppm. The silver content in the ores does not exceed 3.9 ppm, averaging 1.28 ppm. The contents of Cu and Mo in the ores were not determined.

FLUID INCLUSIONS

We performed fluid inclusion (FI) studies of quartz and calcite from gold-bearing sulfide–carbonate–quartz veinlets
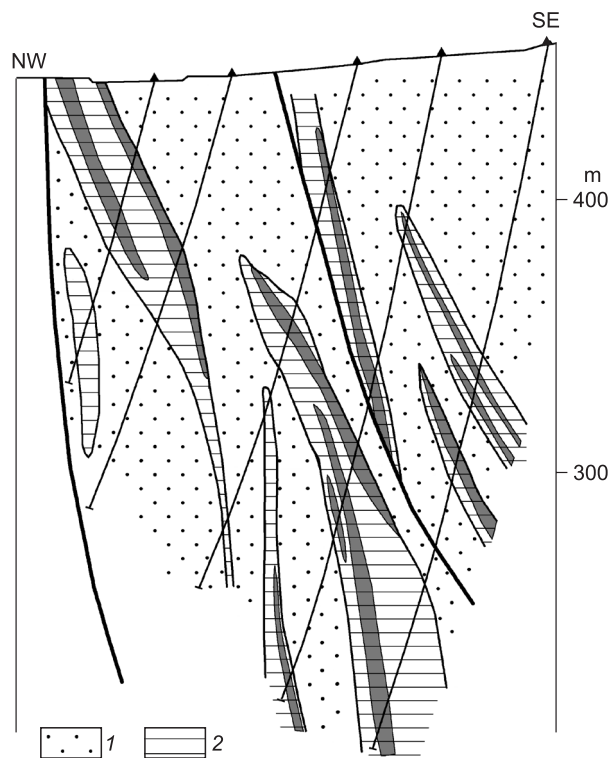
Fig. 3. Metasomatic zoning along the N-7 profile. *1*, pre-ore propylites of the epidote–actinolite facies; *2*, host propylites of the albite–chlorite facies. Other designations follow Fig. 1.

and a Raman spectroscopy analysis of the gas of individual FIs in quartz.

Fluid inclusion analysis was carried out on a Linkam TMS-600 heating/cooling stage with an Olympus BX 51 microscope and LinkSystem 32 DV-NC software in the Laboratory of Thermobarogeochemistry of South Ural State University, Miass (analyst N.N. Ankusheva). The error of measurement was ±0.1 ºC at –20 to 80 ºC and ±1 ºC beyond this temperature range. The salt composition of the fluids was estimated from eutectic temperatures (Davis et al., 1990; Spencer et al., 1990). Homogenization temperatures of FIs were measured at the moment when the vapor bubble disappeared on heating. The concentrations of salts in the fluids were calculated from the final melting points (Bodnar and Vityk, 1994). More than 100 inclusions in quartz and calcite were analyzed. The results were processed using the Statistica 6.1 program.

We studied primary and pseudosecondary biphase FIs 10–20 μm in size, flattened, often elongate, unbranched, with crystallographic faces (Fig. 4) in quartz. The vapor phase reaches 20–30% of the inclusions. There are also secondary inclusions arranged as chains or clusters along quartz cracks. Primary and pseudosecondary inclusions in quartz are similar and contain fluids with eutectic temperatures of –31.0 to –37.8 ºC (n = 80), which indicates $MgCl_2$–NaCl–H_2O fluids. Some inclusions of this association contain fluids with eutectic temperatures of –23 to –24 ºC (n = 15).
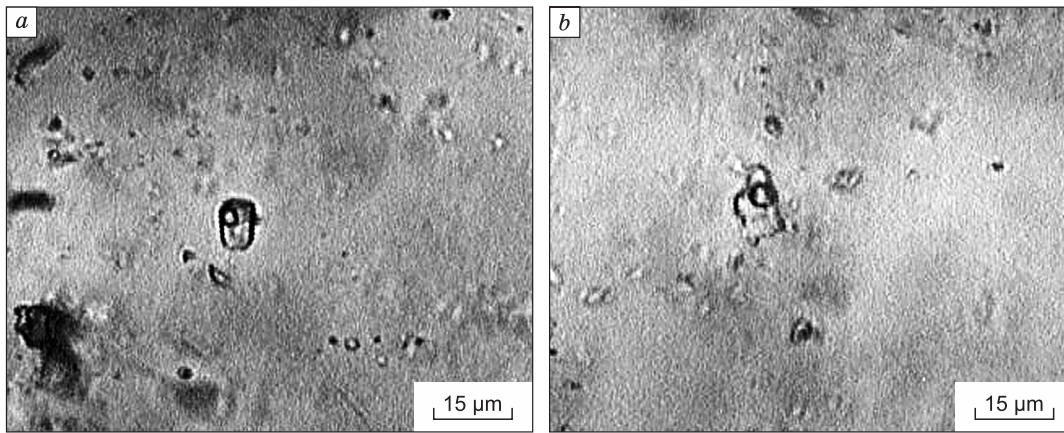
Fig. 4. Fluid inclusions in quartz (*a*) and calcite (*b*).

These temperatures are close to the melting points of the eutectics of NaCl–H_2O fluid with KCl impurity. The salinities (TDS) are 5.8–9.6 wt.% NaCl eqv.; most of the FIs have TDS = 7–8 wt.% NaCl eqv. (the plot in Fig. 5). The inclusions were homogenized into a liquid at 200–260 ºC. The distribution of homogenization temperatures is multimodal, with a wide peak at 230–250 ºC.

Biphase FIs up to 5 μm in size are also revealed in calcite from ore veinlets, which forms cryptocrystalline aggregates and thin veinlets cutting quartz grains (Fig. 4). These inclusions have a rounded shape and form clusters (3–4 inclusions in each). The eutectic temperatures vary from –23.0 to –23.7 ºC ($n = 10$), which indicates NaCl–H_2O fluids with KCl impurity. The TDS of the inclusions is 4.1–6.4 wt.%
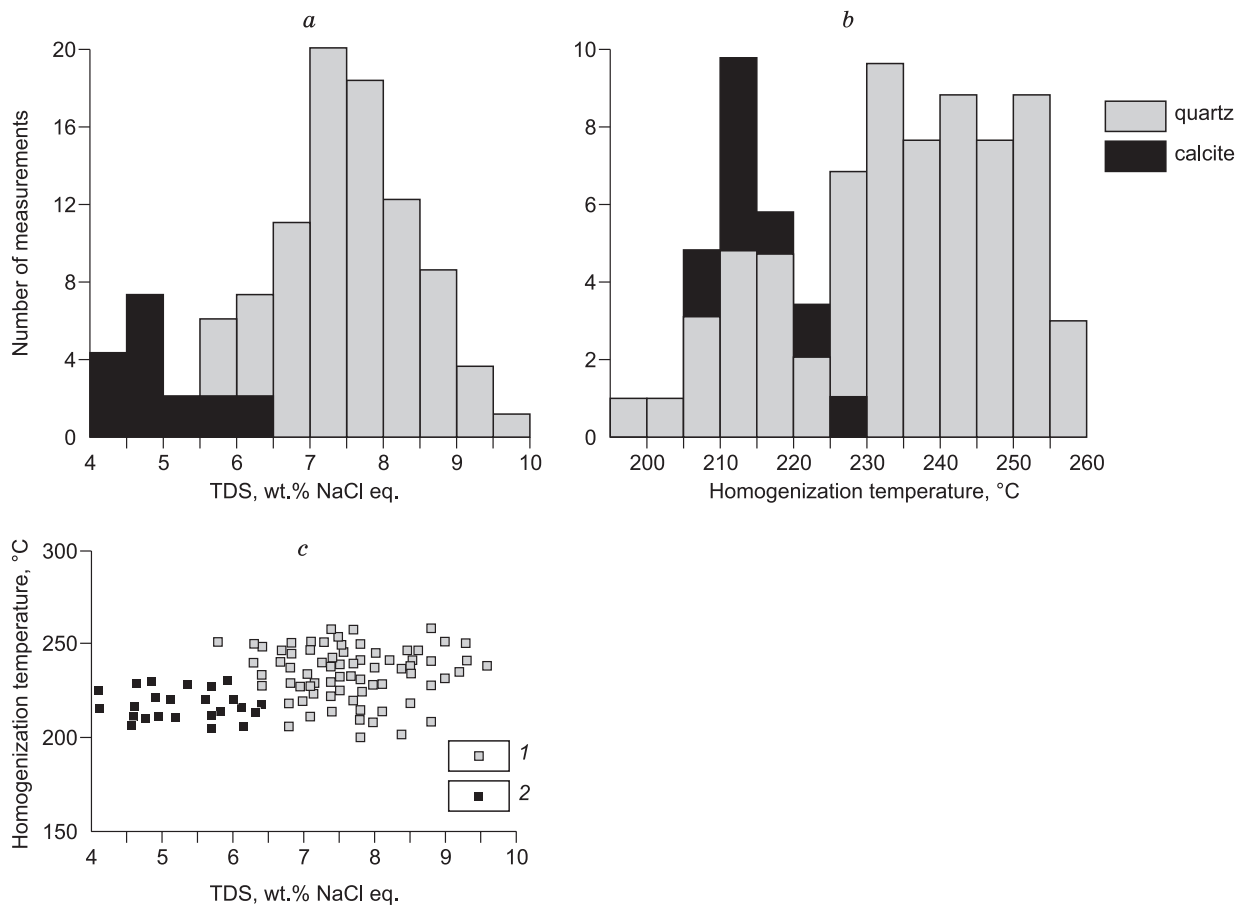
Fig. 5. Results of fluid inclusion study. *a–b*, Distribution of the TDS and T_{hom} values of FIs, *c*, TDS vs. T_{hom} of FIs: *1,* quartz, *2,* calcite.

Table 1. Calculated molar fractions of components, X_a (mol.%), of fluid inclusions in quartz

Sample	$x_{CO_2} \pm \Delta x_{CO_2}$	$X_{N_2} \pm \Delta x_{N_2}$	$x_{CH_4} \pm \Delta x_{CH_4}$
N-5	29.3 ± 9.4	30.5 ± 12.4	40.2 ± 9.9
N-7	34.4 ± 5.5	8.6 ± 4.2	55.4 ± 4.5

NaCl eqv.; most of the FIs have TDS = 4.5–5 wt.% NaCl eqv. (Fig. 5). The homogenization temperatures (T_{hom}) are 205–227 ºC, with a peak falling on 210–215 ºC.

The gas composition of fluid inclusions in quartz. The gas composition of fluids in the inclusions from quartz was determined using a Horiba LabRam HR800 Evolution Raman spectrometer with an Olympus BX-FM microscope (MPlan N ×100 lens), a He–Ne laser (excitation wavelength 514 nm), and a diffraction grating with 1800 gr/mm, operating in confocal mode with a spatial lateral resolution of ~2 μm and a depth resolution of ~3 μm. The analysis was carried out at the Institute of Geology and Geochemistry, Yekaterinburg (analyst E.A. Pankrushina).

The Raman spectra (Burke, 2001) of FIs from quartz showed the presence of CO_2 (29.3–34.4 mol.%), CH_4 (40.2–55.4 mol.%), and N_2 (8.6–30.5 mol.%) (Table 1).

SULFIDE–CARBONATE–QUARTZ VEINLETS

Trace elements in quartz from sulfide–carbonate–quartz veinlets were detected by LA-ICP-MS on an Agilent 7700× mass spectrometer with the MassHunter software and a New Wave Research Up-213 laser attachment at the Institute of Mineralogy, Miass (analyst D.A. Artemyev). Laser parameters: Nd:YAG, radiation wavelength of 213 nm, beam energy of 15–17 J/cm², pulse repetition rate of 10–15 Hz. Laser operation time: 10 s (pre-ablation) + 30 s (blank run) + 60 s (analysis time). Other operating conditions: ablation spot diameter of 100 μm, pre-ablation spot diameter of 110 μm, He as a carrier gas, He flow rate of 0.65 L/min. Mass spectrometer parameters: RF power of 1550 W, Ar as a gas, Ar flow rate of 1.05 L/min. The mass spectrometer was calibrated against multielement solutions. The integration time was 10–30 ms. The NIST SRM-612 and USGS BCR-2g international standard glass samples were used for calibration and calculation. The calculation was made using the Iolite program and ^{29}Si as an internal standard. We studied two samples with five quartz grains in each.

The following trace elements have been identified in quartz: Li, Na, Mg, Al, P, K, Ca, Sc, Ti, V, Cr, Mn, Fe, Ni, Cu, Zn, Ge, As, Sr, Mo, Ag, Cd, Sn, Sb, Ba, W and Pb (Table 2). Major impurities are (ppm) Na (15.7–62.0), Al (11.7–102), P (25.7–38.3), K (4.44–49.0), Ca (33–64), and, in some samples, Fe (up to 113 ppm) and Cu (up to 58 ppm). It was the first LA-ICP-MS analysis of quartz from South Urals gold deposits.

Rare-earth elements and yttrium in calcite from sulfide–carbonate–quartz veinlets were determined by ICP MS on a Perkin Elmer ELAN 9000 mass spectrometer at the Institute of Geology and Geochemistry, Yekaterinburg (analyst D.V. Kiseleva). The element patterns were normalized

Table 2. Contents (ppm) of trace elements in quartz

Element	N-5-1	N-5-2	N-5-3	N-5-4	N-5-5	N-7-1	N-7-2	N-7-3	N-7-4	N-7-5
Li	1.28	2.71	0.81	0.57	1.39	1.04	0.39	0.73	1.09	0.67
Na	35.2	62	24.7	40.7	23.8	21.4	27.2	15.7	46.1	26.5
Mg	2.86	3.25	0.56	1.21	1.93	0.36	3.9	0.53	0.33	1.11
Al	50	55.5	45.8	34.2	54.7	71.8	102	11.7	76.3	12.1
P	36.5	35.8	36.2	35.2	36.9	31.5	29.9	26.5	25.7	38.3
K	19.6	22.8	11.1	14.3	15.8	32.5	49	4.44	37.1	6.49
Ca	49	37	33	37	49	50	64	54	48	44
Sc	2.42	2.4	2.42	2.26	2.37	2.36	2.1	2.24	2.14	2.18
Ti	0.41	0.41	0.36	0.23	0,44	0.33	0.64	0.051	0.197	0.087
V	0.012	0.029	0.003	<0.002	<0.001	<0.004	0.23	0.003	0.003	0.006
Cr	0.72	1.94	0.72	0.48	0.53	0.28	1.23	0.49	0.53	0.5
Mn	0.017	0.008	0.008	0.016	0.03	<0.009	<0.003	0.027	0.055	0.017
Fe	<0.18	<0.13	<0.69	<0.36	0.17	73	113	51,5	55	67.9
Ni	0.51	0.46	0.282	0.36	0,3	0,26	0.28	0.3	0.32	0.33
Cu	0.038	0.148	0.148	0.227	0.093	31	58	23	24.8	37.1
Zn	0.43	0.49	0.136	0.15	0.17	0.56	1.55	0.34	0.36	0.67
Ge	0.47	0.55	0.45	0.48	0.44	1.63	1.46	1.04	1.52	0.95
As	0.62	0.48	0.48	0.7	0.54	1.14	2.77	1.11	1.32	1.24
Sr	0.112	0.052	0.096	0.087	0.106	0.037	0.112	0.048	0.05	0.083
Mo	<0.016	0.001	<0.012	0.003	<0.001	<0.007	0.009	<0.016	<0.012	<0.014
Ag	0	<0.003	0.009	0.006	0.007	0.006	0.052	0.002	0.016	0.084
Cd	0.183	0.049	0.026	0.068	0.043	0.049	0.112	0.047	0.146	0.082
Sn	0.132	0.168	0.184	0.163	0.179	0.144	0.173	0.142	0.107	0.132
Sb	0.175	0.298	0.282	0.215	0.209	0.258	0.138	0.025	0.124	0.062
Ba	1.2	0.72	0.89	0.6	0.85	0.64	1.38	0.19	0.64	0.247
W	0.009	0.013	0.014	0.028	0.003	0.003	0.025	<0.003	0.005	0.013
Pb	0.117	0.119	0.067	0.046	0.043	0.073	0.081	0.037	0.063	0.056

Table 3. REE contents (ppm) in calcite

Element	N-1	N-2	N-3	N-4	N-5	N-6	N-7	N-9	N-10
La	0.04	0.79	0.32	0.31	0.76	0.12	0.1	0.51	0.14
Ce	0.11	1.69	0.58	0.72	1.53	0.19	0.21	0.52	0.19
Pr	0.02	0.26	0.13	0.15	0.27	0.04	0.04	0.17	0.05
Nd	0.12	1.43	0.81	0.86	1.21	0.21	0.22	0.93	0.31
Sm	0.06	0.52	0.33	0.36	0.41	0.07	0.08	0.35	0.13
Eu	0.26	1.25	0.64	0.91	0.42	0.09	0.08	0.39	0.31
Gd	0.15	0.84	0.59	0.60	0.61	0.15	0.1	0.67	0.27
Tb	0.03	0.14	0.11	0.11	0.13	0.03	0.02	0.11	0.05
Dy	0.20	0.99	0.72	0.75	0.95	0.26	0.13	0.76	0.42
Ho	0.05	0.28	0.16	0.16	0.24	0.06	0.03	0.20	0.11
Er	0.17	1.06	0.48	0.43	0.71	0.21	0.08	0.68	0.4
Tm	0.02	0.17	0.07	0.06	0.1	0.03	0.01	0.11	0.07
Yb	0.12	1.25	0.33	0.31	0.76	0.21	0.08	0.78	0.5
Lu	0.06	0.21	0.04	0.04	0.12	0.03	0.01	0.13	0.09
$\sum$REE	1.37	10.88	5.31	5.77	8.22	1.7	1.19	6.31	3.04
La_N/Yb_N	0.24	0.45	0.7	0.72	0.72	0.41	0.9	0.47	0.2
La_N/Sm_N	0.43	0.98	0.63	0.56	1.2	1.11	0.81	0.94	0.69
Gd_N/Yb_N	1.03	0.55	1.48	1.6	0.97	0.59	1.03	0.71	0.45
La_N/Lu_N	0.07	0.4	0.86	0.83	0.68	0.43	1.07	0.42	0.17
Eu/Eu*	5.25	3.94	3.18	3.96	1.99	2.21	2.08	2.18	3.56
Ce/Ce*	0.80	0.82	0.61	0.46	0.82	0.63	0.73	0.39	0.53
Y	1.63	11.64	4.59	8.65	7.03	2.23	0.91	8.69	4.61
Y/Ho	32.6	41.2	28.7	54.1	29.3	37.2	30.3	43.5	41.9

to the chondrite CI (McDonough and Sun, 1995). The Eu and Ce anomalies were calculated by the formulae $Eu/Eu* = Eu_N/(Sm_N/(Tb_N \times Eu_N)^{0.5})^{0.5}$ and $Ce/Ce* = Ce_N/((2La_N + Sm_N)/3)$. The results are as follows (Table 3): $\sum$REE = 1.19–10.88 ppm, Y = 0.91–11.64 ppm, La_N/Yb_N = 0.2–0.9, La_N/Lu_N = 0.07–1.07, Eu/Eu* = 1.99–5.25, Ce/Ce* = 0.39–0.82, and Y/Ho = 28.7–54.1.

Carbon and oxygen isotope compositions of calcite from sulfide–carbonate–quartz veinlets. Analyses were carried out on a DELTA V Advantage mass spectrometer at the Geonauka Common Use Center of the Institute of Geology, Syktyvkar, and on a MAT 253 isotope mass spectrometer at the Analytical Center of the Far East Geological Institute, Vladivostok. The accuracy of $\delta^{13}C$ and $\delta^{18}O$ determination was ±0.2‰ in the former laboratory and ≤0.1‰ in the latter. The obtained $\delta^{13}C$ and $\delta^{18}O$ values (Table 4) are given relative to the PDB and SMOW international stan-

dards, respectively. The carbon and oxygen isotope compositions of the sample N-1 were determined in both laboratories for control of the repeatability of measurements. The differences in the obtained results are close to the analytical error.

The oxygen isotope ratios in calcite from gold-bearing sulfide–carbonate–quartz veinlets vary from 11.9 to 13.9‰, and the carbon isotope ratios, from –5.0 to 0.5‰. The $\delta^{18}O_{H_2O}$ values of the ore-forming fluid, calculated for T_{hom} = 230 °C of FIs in calcite (Zheng, 1999), vary from 3.6 to 5.6‰. The $\delta^{13}C_{CO_2}$ values of the fluid being in equilibrium with calcite at 230 °C (Ohmoto and Rye, 1979) vary from –4.1 to 1.4‰.

Sulfur isotope composition of sulfides from sulfide–carbonate–quartz veinlets. Stable sulfur isotopes were studied in pyrite and arsenopyrite from gold ores (Table 5). The isotope composition of sulfur was determined on a Delta^{PLUS} Advantage mass spectrometer equipped with a Flash EA 1112 element analyzer and a ConFlo IIII interface at the Institute of Mineralogy SU, Miass (analyst S.A. Sadykov). The error in the determination of $\delta^{34}S$ was 0.27‰. The results of measurements are given relative to the CDT interna-

Table 4. Carbon and oxygen isotope compositions of calcite and equilibrium fluid

Sample	$\delta^{13}C$, ‰, PDB	$\delta^{18}O$, ‰, SMOW	$\delta^{13}C_{CO_2}$, ‰, PDB	$\delta^{18}O_{H_2O}$, ‰, SMOW
N-1*	–4.5* (–4.4)	12.1* (12.3)	–3.6* (–3.5)	3.8* (4.0)
N-2*	–2.0	11.9	–1.1	3.6
N-3*	–1.3	13.0	–0.4	4.7
N-4*	0.5	11.9	1.4	3.6
N-16*	–4.0	13.9	–3.1	5.6
N-7	–2.2	12.7	–1.3	4.4
N-13	–5.0	12.5	–4.1	4.2
N-14	–4.4	13.3	–3.5	5.0
N-15	–0.9	13.3	0	5.0

* Analyses were carried out at the Institute of Geology, Syktyvkar; the other analyses, at the Far East Geological Institute, Vladivostok.

Table 5. Sulfur isotope composition of sulfides

Sample	Mineral	$\delta^{34}S$, ‰, CDT
N-5	Pyrite	6.88
N-6	Pyrite	7.40
N-7	Pyrite	9.20
N-8	Pyrite	9.87
N-9	Pyrite	6.95
N-10	Pyrite	6.75
N-12	Pyrite	7.82
N-11	Arsenopyrite	8.70

tional standard. According to the data obtained, the $\delta^{34}S$ is 6.75–9.87‰ in pyrite and 8.7‰ in arsenopyrite.

DISCUSSION AND CONCLUSIONS

The results of fluid inclusion studies show that FIs in quartz from the Nikolaevskoe deposit homogenize at 260–200 °C and FIs in later crystallized calcite, at 227–205 °C. Three-phase inclusions with liquid carbon dioxide were not detected in the studied samples; for this reason, we could not introduce the pressure correction for estimating T_{hom} and determine the true mineral formation temperature. The fluid inclusion data are consistent with the temperature of formation of near-ore propylites of the albite–chlorite facies, 200–250 °C (Zharikov, 1998). Therefore, we think that the T_{hom} of FIs is close to the true mineral formation temperature. In the biotitization zone, the temperature in the wallrock zone was apparently higher. For example, biotite in present-day hydrothermal fluids is stable in the temperature range 280–340 °C (Reyes, 1998). In general, the temperatures of formation of metasomatic wallrocks and carbonate–quartz veinlets correspond to a mesozone. Quartz and calcite were deposited from K–Mg–Na water–chloride fluids with a low TDS (4.1–9.6 wt.% NaCl eqv.). According to Raman spectroscopy data, the mineral-forming fluid contains CO_2, N_2, and CH_4.

The high-sensitivity LA-ICP-MS analysis has shown that ore quartz has low contents of Al (11.7–102 ppm) and Ti (0.051–0.64 ppm). According to the results of modeling (Rusk et al., 2008), the contents of Al in quartz are reflective of the element solubility in the hydrothermal fluid, which is controlled by its pH. At relatively low temperatures, the content of Al tends to decrease as the fluid pH increases. The results of our study suggest that quartz from the Nikolaevskoe deposit crystallized from a weakly acidic low-alumina fluid.
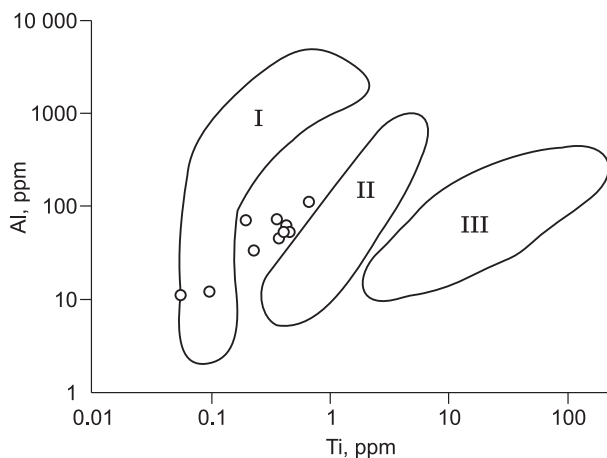
The content of Ti in quartz is a function of the fluid temperature and regularly increases with it (Rusk et al., 2006; Wark and Watson, 2006). It was empirically established that Ti < 10 ppm is typical of hydrothermal quartz formed at <350 °C (Rusk et al., 2008). Apparently, the low contents of Ti in ore quartz from the Nikolaevskoe deposit are much due to the low temperature of its crystallization.

The quantitative ratio of Al and Ti in quartz can be used to assess (tentatively) the type of deposits. Rusk (2012) proposed a diagram for the separation of epithermal, orogenic gold (mesothermal), and porphyry deposits according to this indicative parameter (Fig. 6). In the Al–Ti diagram, the composition points of quartz from the Nikolaevskoe deposit are localized between the fields of mesothermal and epithermal deposits, partly falling into the field of the latter.

The REE and Y patterns of calcite are also informative indicators of hydrothermal ore genesis processes, because these elements have ionic radii close to that of calcium and can substitute it in the crystal lattice of this mineral.

Calcite from the Nikolaevskoe deposit has low REE contents (1.19–10.88 ppm). Its chondrite-normalized REE patterns show accumulation of HREE ($La_N/Yb_N = 0.2–0.9$) (Fig. 7), which is typical of carbonate crystallized from highly alkaline fluid and rich in complexing ligands (Schwinn and Markl, 2005). The La_N/Lu_N values (<1) indicate that complexation played the leading role in REE fractionation (Bau, 1991).

The REE patterns show distinct positive Eu anomalies (1.99–5.25) and negative Ce anomalies (0.39–0.82). The positive Eu anomalies indicate that calcite crystallized from low-temperature (<250 °C) hydrothermal fluid whose REE compositions formed during the rock–fluid interaction under high-temperature conditions (>250 °C) that existed before the calcite crystallization (Bau and Möller 1992; Castorina and Mosi, 2008; Znamenskii et al., 2017), most likely, during the formation of pre-ore actinolite–epidote propylites. At high temperatures, Eu^{2+} was predominant in the fluid; as the temperature decreased, it was oxidized to Eu^{3+}, but the total content of Eu in the fluid remains constant. Ion Eu^{3+} has a

Fig. 6. Al–Ti diagram for quartz from the Nikolaevskoe deposit (light circles). Roman numerals mark the composition fields of ore quartz from epithermal (I), orogenic gold (II), and porphyry (III) deposits (Rusk, 2012).
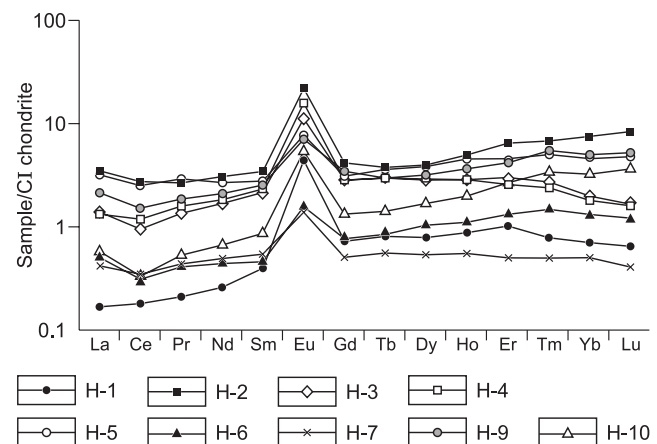
Fig. 7. REE patterns of calcite.

smaller radius than Eu^{2+} and, thus, a higher capacity for incorporation into the calcite crystal lattice. This fact explains the positive Eu anomalies in the REE patterns of calcite.

The positive Eu and negative Ce anomalies indicate a change in the redox environment during the fluid migration and evolution. The negative Ce anomalies might be due to a number of factors. They are probably the result of interaction between the mineral-forming fluid and the marine limestones present in the deposit. Negative Ce anomalies are typical of marine limestones. They were revealed, for example, in the Lower Devonian limestones of the MUF zone (Znamenskii et al., 2013). Such Ce anomalies are preserved during the fluid–limestone interaction (Castorina and Masi, 2008), which leads to LREE depletion of the limestone, because HREE form more stable complex compounds. The HREE enrichment of calcite from the Nikolaevskoe deposit can be an indicator of the above interaction.

Apparently, the hydrothermal system of the deposit included meteoric waters, whose chondrite-normalized REE patterns show negative Ce anomalies (Elderfield et al., 1990).

The Y/Ho ratio in ore minerals gives an insight into the sources of ore-forming fluids (Bau, 1996; Bao et al., 2008). In calcite from the Nikolaevskoe deposit it varies from 28.7 to 54.1. Part of these values falls in the range of the Y/Ho values of magmatic calcite and ore-bearing dolerite-porphyrite and gabbro–diorite-porphyrite dikes of the deposit, and the other values are typical of marine carbonates, including the Lower Devonian limestones of the MUF zone, and seawater (Fig. 8). These data suggest that calcite from the Nikolaevskoe deposit has both magmatic and limestone-extracted components. Apparently, seawater from rock pores also participated in the mineral formation. Volcanic and sedimentary rocks of the deposit accumulated in submarine environment
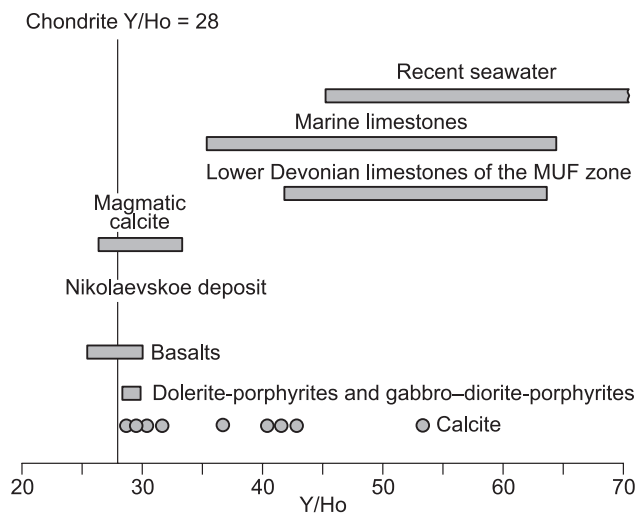
within the ensimatic island arc formed in the Paleo-Ural Ocean basin (Puchkov, 2010). Therefore, the presence of oceanic water in the ore-hosting rocks is highly likely.

The $\delta^{18}O$ and $\delta^{13}C$ values in calcite from the Nikolaevskoe deposit vary from 11.9 to 13.9‰ and from –5.0 to 0.5‰, respectively (Table 4). The model $\delta^{18}O_{H_2O}$ values of the fluid (3.6–5.6‰) being in equilibrium with calcite at 230 ºC (the maximum homogenization temperature of FIs in the mineral) indicate that the mineral (at least during its deposition) contained a mixture of meteoric and magmatic waters (Fig. 9). The slight negative Ce anomalies in the REE patterns of calcite confirm the presence of meteoric water in the fluid.

The carbon isotope composition of CO_2 in the fluid being in equilibrium with calcite at 230 °C shows the participation of not only magmatic carbon ($\delta^{13}C$ = –4.1 to –3.5‰) but also carbon from the host rocks, mostly limestones ($\delta^{13}C$ = –1.3 to 1.4‰), in the ore formation. The results of isotope studies are consistent with the REE and Y patterns of calcite.

The sulfur isotope ratio is 6.75–9.87‰ in pyrite and 8.70‰ in arsenopyrite from the Nikolaevskoe deposit (Table 5). The heavy isotope composition of sulfur might be due to its supply from the host sedimentary rocks and limestones, which contained marine sulfates, or due to the involvement of $[SO_4]^{2-}$ of seawater from the rock pores in the ore genesis. Note that pyrite from the Yubileinoe porphyry gold deposit in the South Urals is also enriched in heavy sulfur isotope (8.5–9.0‰), which indicates an isotope ex-

Fig. 8. Y/Ho in calcite. The Y/Ho values in chondrite, magmatic calcite, marine limestones, and recent seawater (Bau, 1996), in Lower Devonian limestones from the MUF zone (Znamenskii et al., 2013), and in basalts, dolerite-porphyrites, and gabbro–diorite-porphyrites from the Nikolaevskoe deposit (Znamenskiy and Holodnov, 2018).
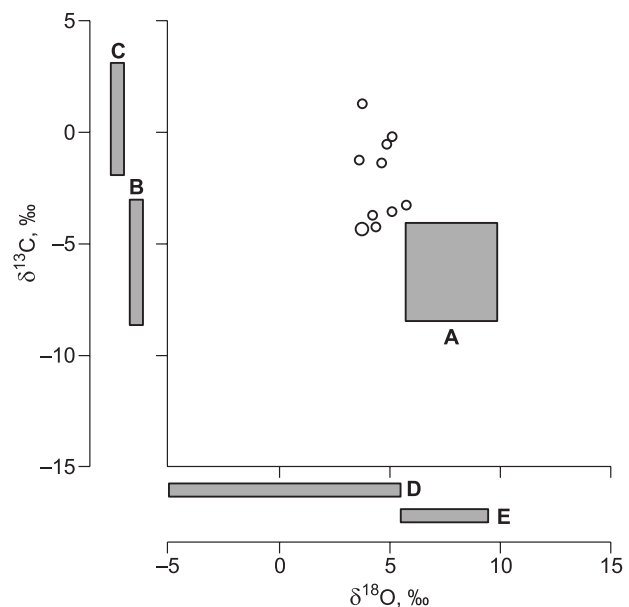
Fig. 9. The carbon and oxygen isotope compositions of the mineral-forming fluid in equilibrium with calcite. A, Field of carbonatites (Keller and Hoefs, 1993); isotope compositions of: B, carbon of magmatic or deep-seated crustal fluid (Taylor, 1986), C, marine limestones, D, oxygen of meteoric water, and E, oxygen of magmatic water (Rollinson, 1993). Light circles mark calcite from the Nikolaevskoe deposit.

change between the fluid and the host rocks. Thus, the gold mineralization of the Nikolaevskoe deposit formed in meso-thermal conditions, with the participation of predominant magmatic fluids and subordinate meteoric water and, most likely, seawater from the rock pores. We have found geo-chemical indicators of the fluid–host-rock interaction. Quartz and calcite of ore veinlets crystallized from K–Mg–Na water–chloride fluids with low TDS. Quartz was depos-ited from weakly acid low-alumina hydrothermal fluids, and calcite, from an HREE-enriched high-alkali fluid. The Niko-laevskoe deposit is similar in formation conditions to (Au ± Cu)–quartz–sulfide deposits transitional between porphyry and epithermal types recognized in island arc porphyry–epi-thermal systems in the southwest of the Pacific ore belt (Corbett and Leach, 1998).

REFERENCES

Bao, S., Zhou, H., Peng, X., Ji, F., Yao, H., 2008. Geochemistry of REE and yttrium in hydrothermal fluids from the Endeavour segment, Juan de Fuca Ridge. Geochem. J. 42 (4), 359–370.

Bau, M., 1991. Rare-earth element mobility during hydrothermal and metamorphic fluid–rock interaction and the significance of oxida-tion state of europium. Chem. Geol. 93 (3–4), 219–230.

Bau, M., 1996. Controls on the fractionation of isovalent trace elements in magmatic and aqueous systems: evidence from Y/Ho, Zr/Hf and lanthanide tetrad effect. Contrib. Mineral. Petrol. 123 (3), 323–333.

Bau, M., Möller, P., 1992. Rare earth element fractionation in meta-morphogenic hydrothermal calcite, magnesite and siderite. Mineral. Petrol. 45 (3–4), 231–246.

Bodnar, R.J., Vityk, M.O., 1994. Interpretation of microthermometric data for H_2O–NaCl fluid inclusions, in: De Vivo, B., Frezzotti, M.L. (Eds.), Fluid Inclusions in Minerals: Methods and Applications. Vir-ginia Polytechnic Institute and State University, Pontignana-Siena, pp. 117–130.

Burke, E.A.J., 2001. Raman microspectrometry of fluid inclusions. Lithos 55 (1–4), 139–158.

Castorina, F., Masi, U., 2008. REE and Nd-isotope evidence for the origin of siderite from the Jebel Awam deposit (Central Morocco). Ore Geol. Rev. 34 (3), 337–342.

Corbett, G.J., Leach, T.M. (Eds.), 1998. Southwest Pacific Rim Gold-Copper Systems: Structure, Alteration and Mineralization. Society of Economic Geologists, Special Publication, No. 6.

Davis, D.W., Lowenstein, T.K., Spenser, R.J., 1990. Melting behavior of fluid inclusions in laboratory-grown halite crystals in the systems $NaCl$–H_2O, $NaCl$–KCl–H_2O, $NaCl$–$MgCl_2$–H_2O, and $CaCl_2$–$NaCl$–H_2O. Geochim. Cosmochim. Acta 54 (3), 591–601.

Elderfield, H., Upstill-Goddard, R., Sholkovitz, E.R., 1990. The rare earth elements in rivers, estuaries, and coastal seas and their signifi-cance to the composition of ocean waters. Geochim. Cosmochim. Acta 54 (4), 971–991.

Grabezhev, A.I., 2009. Sr-Nd-C-O-H-S isotope-geochemical descrip-tion of South Urals porphyry-copper fluid-magmatic systems: Prob-able sources of matter. Litosfera, No. 6, 66–89.

Grabezhev, A.I., 2014. The Yubileinoe porphyry Cu-Au deposit (South Urals, Russia): SHRIMP-II U–Pb zircon age and geochemical fea-tures of ore-bearing granitoids. Dokl. Earth Sci. 454 (1), 72–75.

Grabezhev, A.I., Belgorodskii, E.A., 1992. Productive Granitoids and Metasomatites of Porphyry Copper Deposits [in Russian]. Nauka, Yekaterinburg.

Grabezhev, A.I., Shardakova, G.Yu., Ronkin, Yu.L., Azovskova, O.B., 2017. Systematization of U-Pb zircon ages of granitoids from the copper porphyry deposits on the Urals. Litosfera 17 (5), 113–126.

Keller, J., Hoefs, J. (Eds.), 1995. Carbonatite Volcanism: Oldoinyo Lengai and the Petrogenesis of Natrocarbonatites. Springer, Berlin.

Kosarev, A.M., Puchkov, V.N., Seravkin, I.B., 2005. Petrological-geo-chemical features of the Early Devonian-Eifelian island-arc volca-nics of the Magnitogorsk zone in a geodynamic context. Litosfera, No. 4, 22–41.

Kovalenker, V.A., 2003. Porphyry-epithermal ore-forming systems: contours of problem, in: Proceedings of the International Scientific and Technical Geological Conference "Problems of Ore Deposits and Maximizing the Prospecting Efficiency", Tashkent, 21–24 Oc-tober 2003. IMP, Tashkent, pp. 148–149.

Maslov, V.A., Artyushkova, O.V., 2010. Stratigraphy and Correlation of Devonian Deposits of the Magnitogorsk Megazone in the South Urals [in Russian]. DizainPoligrafServis, Ufa.

McDonough, W.F., Sun, S-S., 1995. The composition of the Earth. Chem. Geol. 120, 223–253.

Ohmoto, H., Rye, R.O., 1979. Isotopes of sulfur and carbon, in: Barner, H.L. (Ed.), Geochemistry of Hydrothermal Ore Deposits. Wiley, New York, pp. 509–567.

Plotinskaya, O.Yu., Grabezhev, A.I., Tessalina, S., Seltmann, R., Gro-znova, E.O., Abramov, S.S., 2017. Porphyry deposits of the Urals: Geological framework and metallogeny. Ore Geol. Rev. 85, 153–173.

Puchkov, V.N., 2010. Geology of the Urals and Cisuralia (Topical Is-sues of Stratigraphy, Tectonics, Geodynamics, and Metallogeny) [in Russian]. DizainPoligrafServis, Ufa.

Reyes, A.G., 1998. Petrology and mineral alteration in hydrothermal systems: From diagenesis to volcanic catastrophes. United Nations University Geothermal Training Programme. Report No. 18.

Rollinson, H.R., 1993. Using Geochemical Data: Evaluation, Presenta-tion, Interpretation. Longman Scientific & Technical, London.

Rusk, B.G., 2012. Cathodoluminescent textures and trace elements in hydrothermal quartz, in: Quartz: Deposits, Mineralogy and Analyt-ics. Springer, New York.

Rusk, B.G., Reed, M.H., Dilles, J., Kent, A., 2006. Intensity of quartz cathodoluminescence and trace-element content of quartz from the porphyry copper deposit at Butte, Montana. Am. Mineral. 91 (8–9), 1300–1312.

Rusk, B.G., Lowers, H.A., Reed, M.H., 2008. Trace elements in hydro-thermal quartz: Relationships to cathodoluminescent textures and insights into vein formation. Geology 36 (7), 547–550.

Schwinn, G., Markl, G., 2005. REE systematics in hydrothermal fluo-rite. Chem. Geol. 216 (3–4), 225–248.

Sillitoe, R.H., 2000. Gold-rich porphyry deposits: descriptive and ge-netic models and their role in exploration and discovery. SEG Rev. 13, 315–345.

Sillitoe, R.H., 2010. Porphyry copper systems. Econ. Geol. 105, 3–41.

Spenser, R.J., Moller, N., Weare, J.H., 1990. The prediction of mineral solubilities in natural waters: A chemical equilibrium model for the Na–K–Ca–Mg–Cl–SO_4 system at temperatures below 25 °C. Geo-chim. Cosmochim. Acta 54 (3), 575–602.

Taylor, B.E., 1986. Magmatic volatiles: Isotopic variation of C, H, and S, in: Valley, J.W., Taylor, H.P., O'Neil, J.R. (Eds.), Stable Isotopes in High Temperature Geological Processes. Mineral. Soc. Am. Rev. Mineral. 16, 185–225.

Wark, D.A., Watson, E.B., 2006. TinaniQ: a titanium-in-quartz geother-mometer. Conrib. Mineral. Petrol. 152 (6), 743–754.

Zharikov, V.A. (Ed.), 1998. Metasomatism and Metasomatic Rocks [in Russian]. Nauchnyi Mir, Moscow.

Zheng, Y.-F., 1999. Oxygen isotope fractionation in carbonate and sul-fate minerals. Geochem. J. 33 (2), 109–126.

Znamenskii, S.E., Michurin, S.V., Ankusheva, N.N., 2013. Generation of ore-forming fluids of the Orlovskoe gold deposit (South Urals). Rudy i Metally, No. 4, 52–60.

Znamenskii, S.E., Ankusheva, N.N., Velivetskaya, T.A., Shanina, S.N., 2017. Composition and sources of mineral-forming fluids of the Orlovka orogenic gold deposit (Southern Urals). Russian Geology and Geophysics (Geologiya i Geofizika) 58 (9), 1070–1079 (1346–1358).

Znamenskiy, S.E., Holodnov, V.V., 2018. Petrological-geochemical features of ore-bearing effusive and intrusive rocks of the Nikolae-vskoe gold-porphyry deposit (the Southern Urals). Litosfera 18 (4), 607–620.

Editorial responsibility: A.S. Borisenko